Title	Transient resonance Raman spectroscopy and density functional theory investigation of iso-polyhalomethanes containing bromine and/or iodine atoms
Author(s)	Zheng, X; Fang, WH; Phillips, DL
Citation	Journal Of Chemical Physics, 2000, v. 113 n. 24, p. 10934-10946
Issued Date	2000
URL	http://hdl.handle.net/10722/42352
Rights	Creative Commons: Attribution 3.0 Hong Kong License

Transient resonance Raman spectroscopy and density functional theory investigation of iso-polyhalomethanes containing bromine and/or iodine atoms

Xuming Zheng, Wei-Hai Fang,[a] and David Lee Phillips[b]
Department of Chemistry, University of Hong Kong, Pokfulam Road, Hong Kong

(Received 11 August 2000; accepted 26 September 2000)

We report additional transient resonance Raman spectra and density functional theory computations for the products formed following ultraviolet photoexcitation of solution phase polyhalomethanes containing bromine and/or iodine atoms. We show that the iso-polyhalomethane photoproduct is responsible for the intense transient absorption band observed in the 350–470 nm region after ultraviolet excitation of polyhalomethanes in the solution phase. We examine the trends and correlation in the density functional theory optimized geometry and intense electronic absorption transition in the 350–470 nm region for the iso-polyhalomethanes containing bromine and/or iodine atoms. We explore the chemical reactivity of the iso-polyhalomethane species using density functional theory computations for the reaction of iso-CH_2Br–Br with ethylene as an example. Our results and comparison with experimental data in the literature indicate that the iso-polyhalomethane species is most likely the methylene transfer agent in the cyclopropanation reactions of olefins using ultraviolet photoexcitation of polyhalomethanes in the solution phase. We briefly discuss the possibility that the photochemistry and chemistry of the iso-polyhalomethanes may give significant release of reactive halogens to the atmosphere. © *2000 American Institute of Physics.* [S0021-9606(00)00148-3]

I. INTRODUCTION

Polyhalomethanes such as CH_2I_2, CH_2BrI, and CH_2Br_2 have been observed in the atmosphere and are potentially significant sources of organoiodine and organobromine compounds emitted into the atmosphere.[1–6] Thus, polyhalomethane photochemical and chemical reactions as well as their lifetimes are of increasing interest in atmospheric chemistry.[1–6] CH_2I_2, CH_2BrI, and CH_2Br_2 have recently had their gas phase ultraviolet–visible absorption spectra measured over the 215–390 nm range and their atmospheric photolysis rates were estimated as a function of altitude and solar zenith angle.[6] Polyhalomethanes are also of interest in a variety of synthetic chemistry reactions such as cyclopropanation reactions of olefins and diiodomethylation of carbonyl compounds.[7–15] Ultraviolet photolysis of CH_2I_2 in the presence of olefins in the solution phase has found utility to produce cyclopropanated products with high stereospecificity.[8–10]

Ultraviolet excitation of polyhalomethanes in the gas phase appears to typically lead to a direct carbon–halogen bond cleavage reaction(s).[16–28] Anisotropy measurements from molecular beam experiments indicate these direct photodissociation reactions usually occur on a time scale much less than a rotational period of the parent molecule.[16,18,19–21] Translational photofragment spectroscopy experiments for CH_2I_2,[18] CH_2BrI,[21] and CF_2I_2,[22,23] showed that the polyatomic photofragments receive substantial amounts of internal excitation of their vibrational and rotational degrees of freedom. Resonance Raman investigations showed several polyhalomethanes have multidimensional reaction coordinates and short-time dynamics qualitatively consistent with a semirigid radical impulsive model of the photodissociation in both the gas and solution phases.[29–38]

Ultraviolet excitation, direct photoionization, and radiolysis of CH_2I_2 in the solution phase all give rise to characteristic absorption bands ~385 nm (strong intensity) and ~570 nm (moderate intensity)[39–45] which have been attributed to several different possible photoproduct species such as trapped electrons,[39] the cation of diiodomethane ($CH_2I_2^+$),[43,45] and the isomer of diiodomethane (iso-CH_2I–I).[41,42] Several femtosecond transient absorption studies examined the photodissociation reaction of CH_2I_2 in the solution phase[46–48] using probe wavelengths of 620 nm,[46] 400 nm,[47] and 290–1220 nm (Ref. 48) to follow the formation and decay of photoproducts. These transient absorption spectra all exhibited similar qualitative features of a fast rise time followed by a fast decay and then a slow rise but three different interpretations were given depending on the assignment of the photoproduct species responsible for the characteristic ~385 nm and ~570 nm absorption bands.[46–48] This uncertainty about the identity of the photoproduct species[38–48] prompted us to use transient resonance Raman experiments and density functional theory computations to better characterize the photoproduct(s).[49] We showed conclusively that the iso-diiodomethane (iso-CH_2I–I) species is the photoproduct responsible for the ~385 nm transient absorption band observed after ultraviolet excitation of diiodomethane in the solution phase.[49] Comparison of these results to those found from gas phase experiments as well as solution phase femtosecond transient absorption experiments

[a]Permanent address: Department of Chemistry, Beijing Normal University, Beijing 100875, People's Republic of China.
[b]Author to whom correspondence should be addressed.

suggest that solvation gives rise to noticeable amounts of the iso-diiodomethane photoproduct by interaction of the initially produced CH_2I and I fragments with the solvent cage around the parent molecule.

Many other polyhalomethane molecules exhibit signature transient absorption bands following excitation in condensed phase[38–45] and we have started to characterize the identity of some of these photoproduct species using a combination of transient resonance Raman spectroscopy and density functional theory computations.[50–52] We found that excitation of either the *A*-band or *B*-band absorption transitions of CHI_3 produced the same iso-CHI_2–I photoproduct species and this suggests that production of iso-polyhalomethane species is not specific to a particular transition and likely occurs generally for $n \rightarrow \sigma^*$ transitions localized on C–X bonds. Our recent observation of the iso-CH_2I–Br species following *A*-band or *B*-band photoexcitation of CH_2BrI (Ref. 51) and the iso-CH_2Br–Br species after ultraviolet photoexcitation of CH_2Br_2 (Ref. 52) in room temperature solutions provide further support for this hypothesis.

In this paper, we report transient resonance Raman spectra and density functional theory calculations for several additional polyhalomethanes. We compare results for seven different polyhalomethanes containing iodine and/or bromine atoms in order to investigate how the iso-polyhalomethane structures and properties vary with different iodine and bromine substitutions. We discuss trends found for the number of iodine and bromine atom substitutions and the relative stability of the iso-polyhalomethane species. We briefly discuss possible implications for cyclopropanation reactions and the chemistry and photochemistry of organoiodine and organobromine compounds in the atmosphere.

II. EXPERIMENT

CBr_4 (99%), CHI_3 (99%), $CHBr_3$ (99+%), CH_2I_2 (99%), CH_2Br_2 (99%), CBr_3F (99+%), CH_2BrI (~97%) and spectroscopic grade cyclohexane solvent (99.9+%) were used to prepare samples (~0.10–0.20 M) for the transient resonance Raman experiments. The experimental apparatus and methods for the nanosecond transient resonance Raman experiments have been previously given[49–56] so only a brief description will be presented here. The pump and probe excitation wavelengths were provided by the hydrogen Raman shifted laser lines and/or harmonics of a Nd:YAG nanosecond pulsed laser. Spectra were acquired using pump–probe time-delays of 0 ns and 10 ns (spectra at both time-delays were similar to one another). A near collinear geometry was used to lightly focus and overlap the pump and probe beams onto a flowing liquid jet of the sample. The Raman scattering signal was collected using a backscattering geometry and reflective optics and then imaged through a depolarizer and entrance slit of a spectrograph. The grating of the spectrograph dispersed the Raman signal onto a liquid nitrogen cooled CCD detector. The Raman signal was sampled for 300–600 s before being read out to an interfaced PC computer and 10–20 of these readouts were added together to obtain the Raman spectrum (pump only, probe-only, pump–probe resonance Raman spectra, and a background spectrum were acquired for each sample). The known vibrational frequencies of the cyclohexane solvent bands were used to calibrate the resonance Raman spectra. The solvent bands and parent compound Raman bands were removed by subtracting the pump-only and probe-only Raman spectra from the pump–probe resonance Raman spectrum so as to obtain the transient resonance Raman spectrum.

III. CALCULATIONS

The Gaussian program package (G98W) was used for all the density functional theory (DFT) calculations[57] and complete geometry optimizations were obtained analytically using C_1 symmetry. B3LYP computations[57,58] were done to find the optimized geometry and vibrational frequencies of the species examined. Time-dependent density functional theory at random phase approximation[59] [TD(RPA)] was used to estimate the electronic transition energies of the species under investigation. The 6-311$G(d,p)$, aug-cc-PVTZ,[60,61] and/or Sadlej-PVTZ (Refs. 62, 63) basis sets were used for the density functional theory computations.

We explored the reactivity of the iso-polyhalomethane species by performing density functional theory (B3LYP with C_1 symmetry) computations for reactions of iso-CH_2Br–Br and CH_2Br radical with ethylene. The complete active space SCF (CASSCF) approach[64–66] was employed for investigation of the dissociation of iso-CH_2Br–Br, since the dissociation involves formation of radicals. An active space with ten electrons in eight orbitals, which originates mainly from 4p electrons of two Br atoms, was used in the CASSCF calculations [hereafter referred to as CAS(10,8)]. Analytic frequency calculations were done in order to confirm the optimized structure as a minimum or first-order saddle point, and to carry out the zero-point energy correction. IRC calculations confirmed the transition state connects the related reactants.[67] The standard 6-31+G* basis set was used for the chemical reaction calculations. We note that relativistic effects may influence the calculated energy of a system that contains heavy atoms, such as Br and I atoms. However, we are concerned about the relative energies (barrier heights and reaction energies) in our chemical reaction computations, and the energy errors originating from relativistic effects will partially cancel out in the calculated relative energies. Thus, we expect that relativistic effects have little influence on the reaction processes investigated here. This is one of the reasons why polarization and diffuse functions were not used for the hydrogen atoms in the chemical reaction computations. Energies of the reactants and products are determined by supermolecule calculations with the intermolecular distance being fixed at 20 Å. In this way, the basis set superposition error is corrected in the computation.

IV. RESULTS AND DISCUSSION

A. Transient resonance Raman spectra, density functional theory computational results, and assignment of iso-polyhalomethane species to the transient resonance Raman spectra

Figure 1 shows the ultraviolet absorption spectra of CH_2Br_2, $CHBr_3$, CBr_4, $CFBr_3$, CH_2I_2, CHI_3, and CH_2BrI in

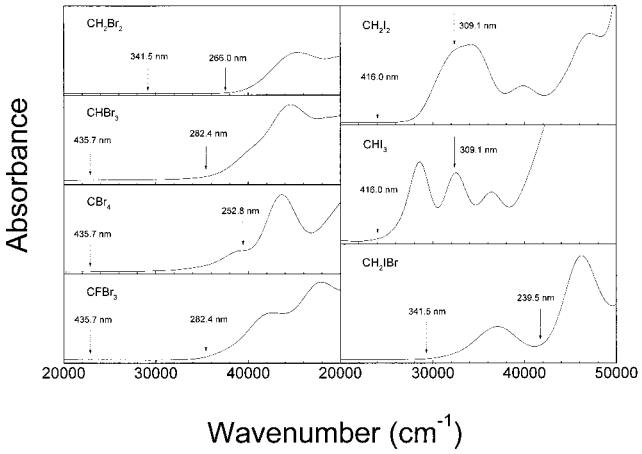

FIG. 1. Absorption spectra of CH_2Br_2, $CHBr_3$, CBr_4, $CFBr_3$, CH_2I_2, CHI_3, and CH_2BrI in cyclohexane solution with the pump (solid arrows) and probe (dashed arrows) excitation wavelengths (in nm) for the transient resonance Raman experiments shown above the spectra.

cyclohexane solution. Figure 2 shows a typical pump only spectrum in the probe wavelength region (A), a probe only resonance Raman spectrum (B), a pump-probe resonance Raman spectrum (C), and the transient resonance Raman spectrum of the $CHBr_3$ photoproduct (D) (obtained after subtraction of the pump only spectrum and the probe only spectrum from the pump–probe resonance Raman spectrum). Figure 3 presents transient resonance Raman spectra of the isomer photoproducts formed from ultraviolet excitation of the seven polyhalomethanes shown in Fig. 1. Since the nanosecond transient absorption spectra in cyclohexane solvent for most of the compounds examined in this study are not known, we did not include any correction of wavelength-

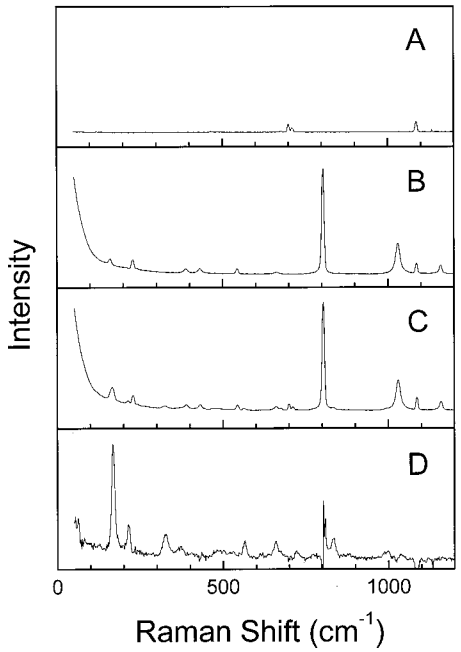

FIG. 2. Example of a pump only 282.4 nm spectrum in the probe wavelength region (A), a probe only 435.7 nm Raman spectrum (B), a pump–probe (282.4 nm/435.7 nm) Raman spectrum (C) and the resulting transient resonance Raman spectrum (D) of the $CHBr_3$ photoproduct.

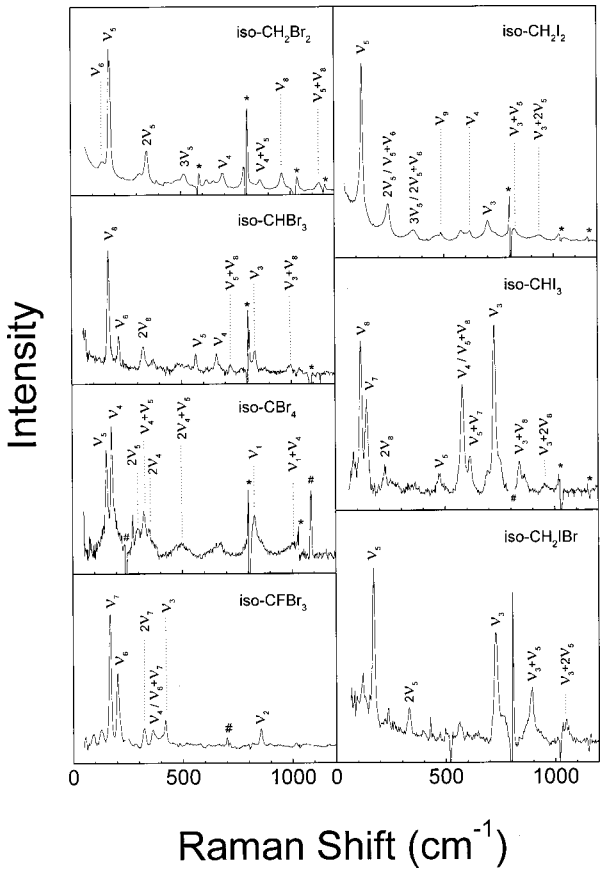

FIG. 3. Transient resonance Raman spectra of iso-CH_2Br_2 (from Ref. 52), iso-$CHBr_3$, iso-CBr_4, iso-$CFBr_3$, iso-CH_2I_2 (from Ref. 49), iso-CHI_3 (from Ref. 50), and iso-CH_2I-Br (from Ref. 51) photoproducts obtained following ultraviolet excitation of the parent compound in cyclohexane solution. The asterisks mark regions where subtraction artifacts are present. The assignments of the larger transient resonance Raman bands are shown above the spectra.

dependent reabsorption in the pump–probe spectra. This could lead to some oversubtraction at large Raman shifts in Figs. 2 and 3. However, most of the resonance Raman bands of interest are found below 1000 cm^{-1} and any effect of oversubtraction on the bands of interest should be small. All of the spectra display most of their intensity in the fundamentals, overtones and combination bands of several Franck–Condon active modes. Density functional theory computations were done for several species that have been proposed as photoproducts for each polyhalomethane system studied so as to elucidate the species mainly responsible for the transient resonance Raman spectra. The DFT computed parameters for the optimized geometry for the iso-polyhalomethane, the polyhalo(or halo)methyl radical fragment and polyhalomethane cation species are given in the supplementary EPAPS material.[68] Table I list the vibrational frequencies obtained from the optimized geometry for each of the proposed species for each molecular system examined in this study and compares them to available vibrational frequencies from resonance Raman and IR experiments. The transient resonance Raman spectra shown in Fig. 3 have fundamental vibrational frequencies that are in good agreement with those predicted for iso-polyhalomethane species but not

TABLE I. Comparison of experimental vibrational frequencies (in cm^{-1}) found from transient resonance Raman spectra and previously reported infrared absorption experiments (Refs. 41 and 42) to the B3LYP calculated vibrational frequencies for the species whose optimized geometry is given in Table I. The corresponding vibrational frequencies for the fully deuterated compounds are given in parentheses.

Ultraviolet excitation of CBr_4						
Resonance Raman Experiment	Iso-CBr_4	B3LYP Calc. 6-311$G(d,p)$	CBr_4^+	B3LYP Calc. 6-311$G(d,p)$	CBr_3	B3LYP Calc. 6-311$G(d,p)$
828	A' ν_1, C–Br Str.	799	A_1 ν_1, Br_1–C–Br_2, Br_3–C–Br_4 sym. str.	585	A_1 ν_1, CBr sym. Str.	313
	ν_2, Br–C–Br wag	350	ν_2, Br–C–Br sym. str.	264	ν_2, C–Br_3 bend.	239
	ν_3, $Br_4Br_3CBr_1$ sym. Str.	277	ν_3, Br–C–Br bend	179	E ν_3, C–Br asym. str	743
179	ν_4, Br_4CBr_3 bend+Br_1–Br_2 str.	175	ν_4, Br_3–C–Br_4 bend	116	ν_4, Br–C–Br bend	159
155	ν_5, Br_1–Br_2 str.+Br_4CBr_3 bend	147	A_2 ν_5, Br_1–C–Br_2, Br_3–C–Br_4 twist	112	CBr_3^+	6-311$G(d,p)$
	ν_6, C–Br_1–Br_2 bend	36	B_1 ν_6, Br_3–C–Br_4 asym. str.	437	A_1 ν_1, CBr sym. Str.	435
	A'' ν_7, Br_4CBr_3 asym. str.	754	ν_7, Br_3–C–Br_4 asym str, Br_1–C–Br_2 wag	155	ν_2, C–Br_3 bend.	315
	ν_8, Br_3CBr_1, Br_4CBr_1 bend	182	B_2 ν_8, Br_1–C–Br_2 asym. str.	734	E ν_3, C–Br asym. str	863
	ν_9, torsion	50	ν_9, Br_1–C–Br_2 rock, Br_3–C–Br_4 wag	176	ν_4, Br–C–Br bend	183

Ultraviolet excitation of $CHBr_3$								
Resonance Raman Experiment	Iso-$CHBr_3$	B3LYP Calc. 6-311$G(d,p)$	$CHBr_3^+$	B3LYP Calc. 6-311$G(d,p)$	$CHBr_2$	B3LYP Calc. 6-311$G(d,p)$	$CHBr_2^+$	B3LYP Calc. 6-311$G(d,p)$
	A' ν_1, C–H stretch	3202	A_1 ν_1, CH str.	3184	A' ν_1, CH str.	3217	A_1 ν_1, CH Str.	3165
	ν_2, C–H scissor	1237	ν_2, Br–C–Br sym. str.	545	ν_2, Br–C–Br sym. str.	615	ν_2, Br–C–Br sym. str.	665
834	ν_3, Br_3CBr_1 asym. str.	848	ν_3, Br–C–Br bend	214	ν_3, CH wag	410	ν_3, Br–C–Br bend	219
658	ν_4, C–H wag	685	E ν_4, Br–C–H scissor	1163	ν_4, Br–C–Br bend	185	B_1 ν_4, C–H def., wag	818
566	ν_5, Br_3–C–Br_1 sym. Str.	581	ν_5, Br–C–Br asym. str.	585	A'' ν_5, BrCH scissor	1190	B_2 ν_5, BrCH scissor	1278
214	ν_6, Br_3–C–Br_1 bend	212	ν_6, Br–C–Br bend	85	ν_6, Br–C–Br asym. str.	757	ν_6, Br–C–Br asym. str.	900
	ν_7, C–Br_1–Br_2 bend	180						
169	ν_8, Br_1–Br_2 str.	159						
	ν_9, torsion	46						

Ultraviolet excitation of $CFBr_3$						
Resonance Raman Experiment	Iso-$CFBr_3$	B3LYP Calc. 6-311$G(d,p)$	$CFBr_3^+$	B3LYP Calc. 6-311$G(d,p)$	$CFBr_2$	B3LYP Calc. 6-311$G(d,p)$
	A' ν_1, C–F stretch	1193	A_1 ν_1, CF str.	1169	A' ν_1, CF Str.	1153
855	ν_2, Br_3CBr_1 asym. str	816	ν_2, Br–C–Br sym. Str.	394	ν_2, Br–C–Br sym. Str.	477
419	ν_3, CF wag	444	ν_3, Br–C–Br bend	206	ν_3, Br–C–F bend	369
362	ν_4, Br_3–C–Br_1 sym. Str.	380	E ν_4, Br–C–F asym. str.	594	ν_4, Br–C–Br bend	170
323	ν_5, Br_3–C–F bend	303	ν_5, Br–C–Br scissor	303	A'' ν_5, Br–C–Br asym. str.	770
204	ν_6, Br_3–C–Br_1 bend	184	ν_6, Br–C–Br bend	72	ν_6, Br–C–F scissor	306
171	ν_7, Br_1–Br_2 str	163				
	ν_8, torsion	80				
	ν_9, C–Br_1–Br_2 bend	41				

Ultraviolet excitation of CH_2Br_2							
Resonance Raman Experiment (from Ref. 52)	Infrared absorption Experiment (from Refs. 41, 42)	Iso-CH_2Br–Br(iso-CD_2Br–Br)	B3LYP Calc. This work 6-311$G(d,p)$	B3LYP Calc. (from Ref. 52) aug-cc-PVTZ	$CH_2Br_2^+$	B3LYP Calc. This work 6-311$G(d,p)$	B3LYP Calc. (from Ref. 52) aug-cc-PVTZ
···	3030 (2213)	A' ν_1, CH_2 sym. Str.	3149	3152 (2275)	A_1 ν_1, CH sym. str.	3131	3132 (2265)
···	1334 (1030)	ν_2, CH_2 scissor	1431	1428 (1078)	ν_2, CH_2 def.	1427	1424 (1045)
···	··· (732)	ν_3, C–Br str.	858	858 (771)	ν_3, CBr sym. Str.	619	626 (596)
690	684 695	ν_4, CH_2 wag	737	738 (594)	ν_4, BrCBr bend	162	169 (168)
176	···	ν_5, Br–Br str.	176	180 (180)	B_1 ν_5, CH asym. str.	3247	3247 (2424)
146	···	ν_6, C–Br–Br bend	130	133 (124)	ν_6, CH_2 rock	878	873 (668)
···	3156 (2384)	A'' ν_7, CH_2 asym. str.	3289	3286 (2456)	A_2 ν_7, CH_2 twist	1042	1032 (732)
960	···	ν_8, CH_2 rock	971	966 (724)	B_2 ν_8, CH_2 wag	1191	1172 (877)
480 ?	···	ν_9, CH_2 twist	461	468 (337)	ν_9, CBr asym. str.	527	528 (507)
			This work	(from Ref. 52)		This work	
		$CH_2Br(CD_2Br)$	6-311$G(d,p)$	aug-cc-PVTZ	CH_2Br^+	6-311$G(d,p)$	
		A_1 ν_1, CH sym. Str.	3168	3172 (2284)	A_1 ν_1, CH sym. Str.	3097	
		ν_2, CH_2 def.	1383	1382 (1029)	ν_2, CH_2 def.	1451	
		ν_3, C–Br str.	696	703 (662)	ν_3, C–Br str.	862	
		B_1 ν_4, CH_2 wag	101	152 (118)	B_1 ν_4, CH_2 def. wag	1095	
		B_2 ν_5, CH asym. Str.	3327	3325 (2488)	B_2 ν_5, CH asym. Str.	3239	
		ν_6, CH_2 rock	930	926 (691)	ν_6, CH_2 rock	983	

TABLE I. (*Continued*.)

Ultraviolet excitation of CHI_3 Resonance Raman Experiment (from Ref. 50)	Iso-CHI_3	B3LYP Calc. (from Ref. 50) Sadlej-PVTZ	CHI_3^+	B3LYP Calc. (from Ref. 50) Sadlej-PVTZ	CHI_2	B3LYP Calc. (from Ref. 50) Sadlej-PVTZ
	A' ν_1, CH str.	3153	A_1 ν_1, CH str.	3150	A' ν_1, CH Str.	3191
	ν_2, CH scissor	1142	ν_2, I–C–I sym. str.	450	ν_2, I–C–I sym. Str.	496
726	ν_3, I–C–I asym. stretch	750	ν_3, I–C–I bend	151	ν_3, I–C–I bend	131
579	ν_4, CH wag	610	E ν_4, I–C–H scissor	1075	ν_4, CH wag	69
477	ν_5, I–C–I asym. stretch	478	ν_5, I–C–I asym. str.	580	A'' ν_5, ICH scissor	1114
	ν_6, I–C–I bend	155	ν_6, I–C–I bend	58	ν_6, I–C–I asym. str.	708
144	ν_7, C–I–I bend	145				
117	ν_8, I–I stretch	119				
	ν_9, torsion	29				

Ultraviolet excitation of CH_2I_2 Resonance Raman Experiment (from Ref. 49)	Infrared absorption Experiment (from Refs. 41, 42)	Iso-CH_2I–I (iso-CD_2I–I)	B3LYP Calc. (from Ref. 49) Sadlej-PVTZ	$CH_2I_2^+$	B3LYP Calc. (from Ref. 49) Sadlej-PVTZ	$CH_2I(CD_2I)$	B3LYP Calc. (from Ref. 49) Sadlej-PVTZ
⋯	3028 (2213)	A' ν_1, CH_2 sym. Str.	3131 (2260)	A_1 ν_1, CH sym. str.	3103 (2246)	A_1 ν_1, CH sym. Str.	3126 (2252)
⋯	1373 (1041–1033)	ν_2, CH_2 scissor	1340 (1011)	ν_2, CH_2 def.	1365 (1003)	ν_2, CH_2 def.	1309 (974)
701 (640)	714/705 (645)	ν_3, C–I str.	755 (645)	ν_3, CI sym. Str.	551 (522)	ν_3, C–I str.	614 (576)
619 (496)	622-611 (498–486)	ν_4, CH_2 wag	619 (476)	ν_4, ICI bend	114 (114)	B_1 ν_4, CH_2 wag	234 (180)
128 (128)	⋯	ν_5, I–I str.	128 (128)	B_1 ν_5, CH asym. str.	3220 (2401)	B_2 ν_5, CH asym. Str.	3288 (2457)
? (~110)	⋯	ν_6, C–I–I bend	99 (93)	ν_6, CH_2 rock	755 (576)	ν_6, CH_2 rock	832 (619)
⋯	3151 (2378)	A'' ν_7, CH_2 asym. str.	3281 (2451)	A_2 ν_7, CH_2 twist	983 (696)		
⋯	⋯	ν_8, CH_2 rock	865 (697)	B_2 ν_8, CH_2 wag	1080 (813)		
487 ?(352 ?)	⋯	ν_9, CH_2 twist	447 (318)	ν_9, CI asym. str.	517 (490)		

Ultraviolet excitation of CH_2IBr Resonance Raman Experiment (from Ref. 51)	Iso-CH_2I–Br (iso-CD_2I–Br)	B3LYP Calc. (from Ref. 51) Sadlej-PVTZ	CH_2BrI^+ (CD_2BrI^+)	B3LYP Calc. (from Ref. 51) Sadlej-PVTZ
	A' ν_1, CH_2 sym. str.	3115 (2251)	A' ν_1 CH_2 sym. Str.	2995 (2172)
	ν_2, CH_2 def.	1357 (1024)	ν_2, CH_2 def.	1283 (937)
730	ν_3, C–I str.	782 (646)	ν_3, CH_2 wag.	1056 (781)
	ν_4, CH_2 wag	671 (541)	ν_4, C–Br str.	659 (629)
173	ν_5, I–Br str.	165 (164)	ν_5, C–I str.	464 (448)
118	ν_6, C–I–Br bend	106 (99)	ν_6, I–C–Br bend	153 (152)
	A'' ν_7, CH_2 asym. str.	3257 (2430)	A'' ν_7, CH_2 asym. str.	3027 (2235)
	ν_8, CH_2 rock	867 (693)	ν_8, CH_2 twist	994 (708)
	ν_9, CH_2 twist	469 (337)	ν_9, CH_2 rock	433 (342)

Infrared Absorption Experiment (from Refs. 41, 42)	Iso-CH_2Br–I (iso-CD_2Br–I)	B3LYP Calc. (from Ref. 51) Sadlej-PVTZ
~3036 (~2222)	A' ν_1, CH_2 sym. Str.	3115 (2248)
⋯ (~1055)	ν_2, CH_2 def.	1377 (1042)
⋯ (~708)	ν_3, C–Br str.	840 (707)
631 (~505)	ν_4, CH_2 wag	698 (560)
	ν_5, I–Br str.	148 (147)
	ν_6, C–I–Br bend	120 (112)
~3165 (~2390)	A'' ν_7, CH_2 asym. str.	3271 (2445)
	ν_8, CH_2 rock	945 (755)
	ν_9, CH_2 twist	429 (309)

the cation or radical fragment species. For example, the transient resonance Raman spectrum for the $CHBr_3$ photoproduct displays fundamental Raman bands at 834 cm^{-1}, 658 cm^{-1}, 566 cm^{-1}, 214 cm^{-1}, and 169 cm^{-1}. These vibrational frequencies are in reasonable agreement with those computed for the iso-$CHBr_3$ species but not for the $CHBr_3^+$ cation or $CHBr_2$ radical fragment species (see Table I). The cation $CHBr_3^+$ has only one A_1 vibrational mode below 250 cm^{-1} (at 214 cm^{-1}) while the experimental spectrum in Fig. 3 clearly shows two fundamentals at 214 cm^{-1} and 169 cm^{-1}

(which also display a combination band with one another). In addition, the cation $CHBr_3^+$ has only one A_1 vibrational mode in the 500–850 cm^{-1} region (at 545 cm^{-1}) while the experimental spectrum in Fig. 3 clearly shows three fundamentals at 566 cm^{-1}, 658 cm^{-1}, and 834 cm^{-1}. Thus, we can rule out the $CHBr_3^+$ cation as the species responsible for the transient resonance Raman spectrum of the $CHBr_3$ photoproduct. The $CHBr_2$ radical fragment also displays only one A_1 fundamental in the 500–850 cm^{-1} region (at 615 cm^{-1}) and one fundamental in the 100–250 cm^{-1} region (at 185 cm^{-1}). The $CHBr_2$ radical fragment can also be ruled out as the species responsible for the transient resonance Raman spectrum of the bromoform photoproduct which clearly has fundamental bands at 169 cm^{-1}, 214 cm^{-1}, 566 cm^{-1}, 658 cm^{-1}, and 834 cm^{-1}. The $CHBr_2^+$ cation exhibits computed vibrational frequencies (see Table I) similar to those for the $CHBr_2$ radical and can likewise be ruled out as the photoproduct species. The radical fragment species (like CH_2X, CHX_2, and CX_3) have structures and vibrational frequencies similar to those for the corresponding cation fragment species (like CH_2X^+, CHX_2^+, and CX_3^+). This and the fact that none of the radical fragment species can be assigned to the observed photoproduct species makes it highly unlikely the cation fragment is responsible for the transient resonance Raman spectra observed in Fig. 3. Thus, we only computed optimized structures and vibrational frequencies for selected cation fragment species ($CHBr_2^+$, CH_2Br^+, and CBr_3^+) for comparison purposes. Similar arguments to those given above for possible $CHBr_3$ photoproduct species indicate that all of the transient resonance Raman spectra for polyhalomethane photoproducts shown in Fig. 3 belong to iso-polyhalomethane species and not the parent molecule cation species or the radical (or cation) fragment species. Figure 4 shows schematic diagrams of the structures of the eight iso-polyhalomethane species investigated in this paper. Inspection of Table I shows that the iso-polyhalomethane species containing iodine and/or bromine atoms generally have two or more vibrational modes with A_1 or A' symmetry in the 100–200 cm^{-1} region associated with the halogen–halogen (X–X) stretch and carbon–halogen–halogen (C–X–X) bend motions. The Br–C–Br bend is involved sometimes in the case of the more highly substituted iso-CBr_4 and iso-$CFBr_3$ species. The presence of two or more A_1 or A' vibrational fundamentals in the 100–200 cm^{-1} region of the resonance Raman spectra appears indicative of the polyhalomethane isomer species that contain a carbon–halogen–halogen (C–X–X) structure. These modes generally display strong overtones and/or combination bands with other Franck–Condon active modes in the resonance Raman spectra of Fig. 3. This indicates the strong transient absorption bands in the 350–470 nm region for the isomer photoproducts are associated with the C–X–X chromophore (where X=Br and/or I).

B3LYP/3-21G* time-dependent random phase approximation (TD/RPA) computations to estimate the electronic transition energies have been done previously for CH_2I_2 and reasonable agreement was obtained between the computed and experimental values.[69] Results for similar computations are shown in Table II for the isomer, cation, and radical fragment species that have been proposed as photoproducts

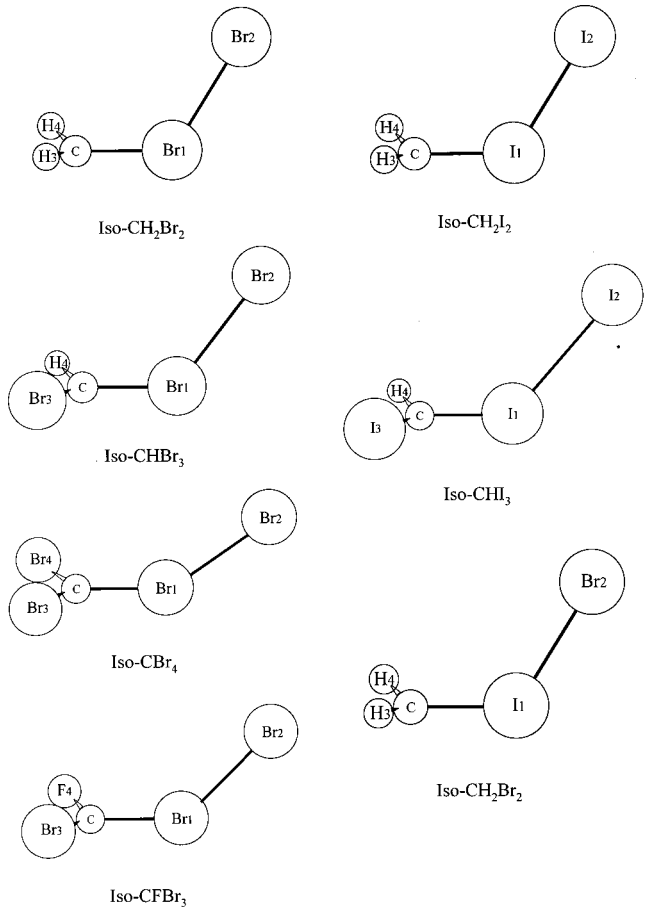

FIG. 4. Schematic diagram showing the computed optimized geometry for the iso-CH_2Br–Br, iso-$CHBr_3$, iso-CBr_4, iso-$CFBr_3$, iso-CH_2I–I, iso–iso-CHI_3, and iso-CH_2I–Br photoproduct species observed experimentally in room temperature solutions (cyclohexane solvent). The B3LYP/6-311G(d,p) computed values for the C–Br bond length, Br–Br bond length, and C–Br–Br angle are 1.774 Å, 2.699 Å, and 123.2° for iso-CH_2Br–Br, 1.791 Å, 2.720 Å, and 128.4° for iso-$CHBr_3$, 1.837 Å, 2.706 Å, and 139.3° for iso-CBr_4, and 1.888 Å, 2.651 Å, and 149.1° for iso-$CFBr_3$. The B3LYP/Sadlej-PVTZ computed values for the C–I bond length, I–I (or I–Br) bond length and C–I–I (or C–I–Br) angle are 1.957 Å, 3.042 Å, and 118.2° for iso-CH_2I–I, 2.000 Å, 3.036 Å, and 128.8° for iso-CHI_3, and 1.960 Å, 2.790 Å, and 121.0° for iso-CH_2I–Br.

from ultraviolet photoexcitation of polyhalomethanes in condensed phase environments. The polyhalomethane isomer species have computed singlet transitions in the 350–470 nm region with strong oscillator strengths (iso-CBr_4 at 454 nm with 0.4511 oscillator strength, iso-$CHBr_3$ at 395 nm with 0.5952 oscillator strength, iso-$CFBr_3$ at 400 nm with 0.4070 oscillator strength, iso-CH_2Br_2 at 358 nm with 0.5883 oscillator strength, iso-CHI_3 at 465 nm with 0.5096 oscillator strength, iso-CH_2I_2 at 425 nm with 0.4023 oscillator strength, iso-CH_2I-Br at 358 nm with 0.4582 oscillator strength, and iso-CH_2Br-I at 422 nm with 0.5317 oscillator strength). These strong electronic transitions show a reasonable correlation with the strong experimental transient absorption bands reported earlier for photoproducts formed after photoexcitation of polyhalomethanes in low temperature solids.[39–45] For example, Simon and Tatham[39] observed intense experimental absorption bands at ~504 nm for CBr_4 photoproduct, ~446 nm for the $CHBr_3$ photoproduct, ~390

TABLE II. Electronic absorption transition energies (singlet transitions) obtained from density functional theory calculations for the species whose optimized geometry is listed in the EPAPS and whose computed vibrational frequencies are given in Table I. The calculated oscillator strengths are given in parentheses.

Intense absorption band in the 350–550 nm region Experiment λ_{max}	URPA//UB3LYP/			
	Iso-CBr_4	CBr_4^+	CBr_3	CBr_3^+
	6-311$G(d,p)$	6-311$G(d,p)$	6-311$G(d,p)$	6-311$G(d,p)$
504 nm (from Ref. 39)	454 nm (0.4511)	1985 nm (0.1078)	330 nm (0.0000)	290 nm (0.0000)
	434 nm (0.0001)	926 nm (0.0001)	250 nm (0.0000)	254 nm (0.0000)
	413 nm (0.0187)	618 nm (0.0000)	243 nm (0.0004)	228 nm (0.1723)
	272 nm (0.2247)	519 nm (0.0011)	227 nm (0.0035)	
	259 nm (0.0003)	314 nm (0.0002)		
	230 nm (0.0002)	306 nm (0.121)		
	Iso-$CHBr_3$	$CHBr_3^+$	$CHBr_2$	$CHBr_2^+$
	6-311$G(d,p)$	6-311$G(d,p)$	6-311$G(d,p)$	6-311$G(d,p)$
	427 nm (0.0005)	1296 nm (0.0000)	289 nm (0.0006)	303 nm (0.0000)
446 nm (from Ref. 39)	407 nm (0.0307)	1260 nm (0.0100)	223 nm (0.0010)	280.3 nm (0.0000)
	395 nm (0.5952)	288 nm (0.0336)	217 nm (0.0021)	279.6 nm (0.0002)
	251 nm (0.0003)		205 nm (0.0001)	230 nm (0.2449)
	239 nm (0.1073)		184 nm (0.0281)	
	220 nm (0.0475)		183 nm (0.0006)	
		Iso-$CFBr_3$	$CFBr_3^+$	$CFBr_2$
	6-311$G(d,p)$	aug-cc-PVTZ	6-311$G(d,p)$	6-311$G(d,p)$
	400 nm (0.4070)	398 nm (0.4318)	1447 nm (0.0069)	276 nm (0.0038)
	378 nm (0.0188)	362 nm (0.0082)	654 nm (0.0000)	235 nm (0.0000)
	364 nm (0.0044)	345 nm (0.0031)	349 nm (0.0336)	227 nm (0.0009)
	240 nm (0.2555)	241 nm (0.2197)		209 nm (0.0000)
	235 nm (0.1249)	232 nm (0.0503)		203 nm (0.0249)
	225 nm (0.0451)	212 nm (0.0200)		183 nm (0.0382)
		Iso-CH_2Br_2		$CH_2Br_2^+$
	6-311$G(d,p)$ (this work)	aug-cc-PVTZ (from Ref. 52)	6-311$G(d,p)$ (this work)	aug-cc-PVTZ (from Ref. 52)
	410 nm (0.0001)	390 nm (0.0002)	2333 nm (0.1296)	1941 nm (0.1150)
390 nm (from Ref. 39)	386 nm (0.0248)	374 nm (0.3380)	894 nm (0.0003)	814 nm (0.0003)
360 nm (from Ref. 42)	358 nm (0.5883)	356 nm (0.1919)	706 nm (0.0000)	644 nm (0.0000)
	252 nm (0.0000)	249 nm (0.0001)	305 nm (0.0004)	298 nm (0.0001)
	203 nm (0.0600)	219 nm (0.0033)	219 nm (0.0625)	216 nm (0.0462)
	172 nm (0.0744)	201 nm (0.1005)		
		CH_2Br		CH_2Br^+
	6-311$G(d,p)$ (this work)	aug-cc-PVTZ (from Ref. 52))		6-311$G(d,p)$
	252 nm (0.0001)	255 nm (0.0011)		316 nm (0.0000)
	193 nm (0.0000)	198 nm (0.0001)		197 nm (0.1713)
	181 nm (0.0000)	194 nm (0.0000)		180 nm (0.0009)
	Iso-CHI_3	CHI_3^+		CHI_2
	Sadlej-PVTZ	Sadlej-PVTZ		Sadlej-PVTZ
	(from Ref. 50)	(from Ref. 50)		(from Ref. 50)
445 nm (from Ref. 39)	465 nm (0.5096)	1264 nm (0.0096)		398 nm (0.0000)
	452 nm (0.0134)	405 nm (0.0006)		308 nm (0.0000); 301 nm (0.0000);
	414 nm (0.0045)	322 nm (0.0002)		298 nm (0.0000); 236 nm (0.0006);
	324 nm (0.1408)	1190 nm (0.0000)		232 nm (0.0068); 227 nm (0.0006);
	293 nm (0.0064)	327 nm (0.0001)		218 nm (0.0010); 214 nm (0.0131);
				212 nm (0.0381)
	Iso-CH_2I_2	$CH_2I_2^+$		CH_2I
	Sadlej-PVTZ	Sadlej-PVTZ		Sadlej-PVTZ
	(from Ref. 49)	(from Ref. 49)		(from Ref. 49)
380 nm (from Ref. 39)	443 nm (0.0002)	2648 nm (0.1250)		316 nm (0.0001)
385 nm (from Refs. 41, 42)	425 nm (0.4023)	1004 nm (0.0003)		262 nm (0.0001)
	404 nm (0.0772)	753 nm (0.0000)		216 nm (0.0009)
	284 nm (0.0002)	341 nm (0.0003)		
	280 nm (0.0230)			
	208 nm (0.0671)			

TABLE II. (*Continued*.)

Intense absorption band in the 350–550 nm region Experiment λ_{max}	URPA//UB3LYP/		
	Iso-CH_2I–Br Sadlej-PVTZ (from Ref. 51)	Iso-CH_2Br–I Sadlej-PVTZ (from Ref. 51)	CH_2BrI^+ Sadlej-PVTZ (from Ref. 51)
403 nm (Refs. 41, 42 for iso-CH_2Br–I)	373.14 nm (0.0005)	493.72 nm (0.0000)	486 nm (0.0017)
	358.45 nm (0.4582)	473.45 nm (0.0308)	314 nm (0.0021)
	320.19 nm (0.0166)	422.43 nm (0.5317)	276 nm (0.0003)
	318.91 nm (0.0000)	304.59 nm (0.0000)	254 nm (0.0000)
	302.22 nm (0.0000)	302.00 nm (0.0000)	246 nm (0.0001)
	280.54 nm (0.0000)	264.94 nm (0.0000)	
	260.51 nm (0.0002)	262.18 nm (0.0006)	
	250.04 nm (0.0240)	238.95 nm (0.0009)	
	210.52 nm (0.0770)	213.48 nm (0.1242)	

nm for the CH_2Br_2 photoproduct, ~445 nm for the CHI_3 photoproduct, and ~380 nm for the CH_2I_2 photoproduct in a 77 K isopentane–methylcyclohexane glass. However, the cation and radical fragment species generally do not exhibit computed strong electronic transitions in the 350–470 nm region. This provides further support for our assignment of the iso-polyhalomethane species as the photoproducts responsible for the intense transient absorption bands[39–45] and the transient resonance Raman spectra of Fig. 3.

B. Trends observed in iso-polyhalomethanes containing bromine and/or iodine

The optimized geometry for the iso-CH_2Br-Br, iso-$CHBr_3$, iso-CBr_4, and iso-$CFBr_3$ species [using the same 6-311G(d,p) computations across this series of compounds] and the iso-CH_2I–I and iso-CHI_3 species (using the sadlej-PVTZ basis set) shows some interesting trends. As the number of Br atoms increases, the C–Br_1–Br_2 angle and the C–Br_1 bond length increase noticeably from 123.2° and 1.774 Å in iso-CH_2Br–Br to 139.3° and 1.837 Å in iso-CBr_4. However, the Br_1–Br_2 bond length stays in a narrow range for the iso-CH_2Br–Br, iso-$CHBr_3$ and iso-CBr_4 species (2.699 Å, 2.720 Å, and 2.706 Å, respectively). This suggests that replacement of the hydrogen atoms by bromine atoms results in somewhat weaker C–Br bonds and some crowding of the terminal Br_2 atom so that the C–Br_1–Br_2 angle increases without affecting the Br_1–Br_2 bond very much. This also appears to be the situation for replacement of a hydrogen atom by an iodine atom in the iodine containing polyhalomethanes: the C–I_1–I_2 angle and the C–I_1 bond length increase noticeably from 118.2° and 1.957 Å in iso-CH_2I-I to 128.8° and 2.000 Å in iso-CHI_3, while the I_1–I_2 bond length stays in a narrow range (3.042 Å and 3.036 Å, respectively). Upon going from the dihalomethane to the haloform, there is a larger change in the C–X_1–X_2 angle and C–X_1 bond length for the iodine compounds (+10.6° and +0.043 Å) compared to the bromine compounds (+5.2° and +0.017 Å). This suggests that steric effects and the polarizability of the replacement atom are mostly responsible for this substituent effect (at least in bromine and iodine containing polyhalomethanes). These trends in the C–X_1–X_2 angle and C–X_1 bond length for the iodine and bromine containing compounds exhibit some correlation with the transition energy of the intense transitions in the 350–470 nm region computed for these compounds in Table II. For example, as the number of Br atoms increases the most intense electronic transition shifts from 358 nm for iso-CH_2Br–Br to 395 nm for iso-$CHBr_3$ to 454 nm for iso-CBr_4. This also occurs for iodine containing polyhalomethanes: 425 nm for iso-CH_2I–I and 465 nm for iso-CHI_3. Each additional bromine or iodine atom appears to red shift the most intense electronic transition ~40 to 60 nm. The isomer species containing Br atoms have transitions that are blue shifted ~60 nm or so compared to the corresponding iodine containing polyhalomethanes. This appears to be due to the influence of the C–Br vs the C–I part of the C–X–X chromophore. The bromoiodomethane isomers, iso-CH_2I–Br and iso-CH_2Br–I, do not follow the expected trend for their absorption band position: one may expect that the isomer containing the C–I bond should be at a longer the wavelength compared to the isomer containing the C–Br bond. To better understand this paradox, it is useful to consider the halogen-halogen bond lengths in comparison to the isomer species containing only bromine or iodine atoms. The I–Br bond length is computed to be 2.790 Å in iso-CH_2I–Br. This value is closer to a Br–Br bond length (~2.70 Å) found in the iso-polyhalomethanes containing bromine atoms while the Br–I bond length is computed to be 2.926 Å in iso-CH_2Br–I which is closer to a I–I bond length (~3.04 Å) found in the iso-polyhalomethanes containing iodine atoms. Since the I–Br bond length is close to that for the Br–Br bond length then the energy of the intense electronic transition for iso-CH_2I–Br should be similar to that found for iso-CH_2Br–Br. Since the Br–I bond length is close to that for the I–I bond length then the intense electronic transition for iso-CH_2Br–I should be similar to that found for iso-CH_2I–I. This is indeed the case, the 358 nm strong transition of iso-CH_2I–Br is similar in energy to the ~358 nm strong transition of iso-CH_2Br–Br and the 422 nm strong transition of iso-CH_2Br–I is close to that of the 425 nm strong transition of iso-CH_2I–I. Thus, it appears that halogen–halogen part of the C–X–X chromophore is more important in determining the electronic transition energy than the C–X bond length and the C–X–X bend angle al-

though these are also important. This is consistent with the intensity pattern of the Franck–Condon active modes found in the transient resonance Raman spectra of Fig. 3. The transient resonance Raman spectra show that the halogen–halogen stretch vibrational modes are generally the most intense progression and usually form combination bands with the Franck–Condon active modes associated with the C–X–X bend and C–X motions.

Replacement of a hydrogen atom in iso-$CHBr_3$ to give iso-$CFBr_3$ results in intriguing changes in the computed geometry. First, the C–Br_1 bond in iso-$CFBr_3$ (~1.888 Å) is weakened further than in iso-CBr_4 (~1.837 Å) and the C–Br_1–Br_2 bend angle increases further in iso-$CFBr_3$ (to ~149.1°) than in iso-CBr_4 (to ~139.3°). In addition, the Br_1–Br_2 bond becomes noticeably stronger in iso-$CFBr_3$ (to ~2.651 Å) while the Br_1–Br_2 bond remains almost the same in iso-CBr_4, iso-$CHBr_3$, and iso-CH_2Br–Br (2.706 Å, 2.720 Å, and 2.699 Å, respectively). This indicates that replacement of a hydrogen atom by a fluorine atom results in somewhat different behavior than replacement of a hydrogen atom by a bromine atom or an iodine atom in the iso-polyhalomethanes. The smaller and substantially more electronegative fluorine atom appears to perturb the iso-polyhalomethane structure more through the bonds (i.e., the C–X and X–X bonds and hence the C–X–X angle as well). However, the larger and less electronegative but more polarizable bromine and iodine atoms perturb the iso-polyhalomethane structure more through steric and dispersion effects (i.e., mainly affects the C–X bond and C–X–X angle but not very much effect on the X–X bond).

It is also intriguing that the computed intense electronic transition energy only shifts to ~400 nm for iso-$CFBr_3$ compared to ~454 nm for iso-CBr_4 and ~395 nm for iso-$CHBr_3$. As one goes from iso-CH_2Br–Br to iso-$CHBr_3$ to iso-CBr_4 the C–Br bond becomes longer and the C–Br–Br angle larger while the Br–Br bond length is about the same and the intense electronic transition energy shifts from 358 nm to 395 nm to 454 nm (see Table II). Since the C–Br bond length and the C–Br–Br bond angles are even larger for the iso-$CFBr_3$ species compared to the iso-CBr_4 species, one might expect that the transition energy of the intense absorption band for iso-$CFBr_3$ should be even more red shifted compared to the iso-CBr_4 species. Why is this not the case? It is important to remember that there is a very strong correlation of the halogen–halogen bond length with the position of the strong electronic absorption band associated with the C–X–X chromophore (see our preceding discussion of the two iso-bromoiodomethane species). The iso-$CFBr_3$ species has a noticeably stronger Br–Br bond (~2.651 Å) compared to iso-CBr_4 (~2.706 Å) and this probably blue shifts the intense electronic absorption associated with the C–X–X chromophore. This appears to illustrate competition between the C–X bond length, the C–X–X bond angle and the X–X bond length in determining the position of the intense electronic transition associated with the C–X–X chromophore in the iso-polyhalomethane species. Our preliminary results indicate that fluorine containing iso-polyhalomethane species will likely have a stronger halogen–halogen bond than the corresponding iso-polyhalomethane species that does not contain fluorine. This may cause the position of the intense electronic transition associated with the C–X–X chromophore to be blue shifted from the position expected based only on the changes in the C–X bond length and C–X–X angle upon iodine and/or bromine atom substitution.

TABLE III. Energies for iso-polyhalomethanes shown in Table I relative to parent molecules found from the BLYP density functional theory computations. ΔE = energy difference between isomer molecule and corresponding parent molecule.

Species	ΔE
Iodine containing polyhalomethanes (from B3LYP/sadlej-PVTZ computations)	
iso-CHI_3	30.8 kcal/mol
iso-CH_2I–I	40.3 kcal/mol
iso-CH_2I–Br	43.0 kcal/mol
iso-CH_2Br–I	47.1 kcal/mol
Bromine containing polyhalomethanes [from B3LYP/6-311G(d,p) computations]	
iso-CBr_4	32.8 kcal/mol
iso-$CHBr_3$	42.7 kcal/mol
iso-$CFBr_3$	39.6 kcal/mol
iso-CH_2Br–Br	51.3 kcal/mol

We have performed density functional theory computations to explore the stability of the iso-polyhalomethane relative to the parent polyhalomethane and these results are shown in Table III. When the number of iodine or bromine atoms increase, the energy of the iso-polyhalomethane species decreases and becomes closer to that of the parent compound. For example as one goes from iso-CH_2I_2 to iso-CHI_3, the ΔE relative to the parent molecule goes from 40.3 kcal/mol for iso-CH_2I–I to 30.8 kcal for iso-CHI_3. There is a similar trend for the bromine species ΔE: 51.3 kcal/mol for iso-CH_2Br–Br, 42.7 kcal/mol for iso-$CHBr_3$ and 32.8 kcal/mol for iso-CBr_4. As the halogen atom species changes from iodine to bromine, the energy of the isomer becomes larger (for example changing from iso-diiodomethane with $\Delta E = 40.3$ kcal/mol to iso-dibromomethane with $\Delta E = 51.3$ kcal/mol). Addition of fluorine appears to only moderately lower ΔE (compare iso-$CFBr_3$ to iso-$CHBr_3$ in Table III). The number and identity of the halogen atoms in iso-polyhalomethanes significantly changes their stability relative to the parent polyhalomethane species. We note the caveat that the computed values are for isolated molecules and it is unclear how much solvent effects will change these values.

C. Implications for cyclopropanation reactions of olefins via ultraviolet photoexcitation of polyhalomethanes in the presence of olefins

There is some evidence in the literature[70] that iso-polyhalomethanes react with olefins. Brown and Simons[70] noted that ultraviolet excitation of polyhalomethanes produced ''color centers'' that had characteristic intense transient absorption bands in the 350–470 nm region. When trace amounts of olefins were added and the 77 K matrix allowed to warm up then new transient absorption bands ~310–320 nm appeared with clean isobestic points from the

''color centers'' transient absorption bands (see Figs. 4 and 5 in Ref. 70). These new transient absorption bands ~310 to 320 nm were convincingly assigned to halogen molecule-olefin species (such as I_2–olefin and Br_2–olefin complexes).[70] The new transient absorption bands ~310–320 nm also do not appear when the olefins are not present. No Br_2 was produced from ultraviolet excitation of polybromomethanes in the absence of olefins.[70] We have shown that these ''color center'' intense transient absorption bands in the 350–470 nm region are really due to the iso-polyhalomethane species (this work and Refs. 49–52) for many of the polyhalomethanes examined including $CHBr_3$ (this work), CH_2Br_2,[52] and CH_2I_2.[49] This combined with the previous experiments of Brown and Simons[70] indicates that iso-polyhalomethanes readily react with olefins to give a halogen molecule product which then forms a halogen molecule–olefin complex. The following reaction scheme (using CH_2I_2 and CH_2Br_2 as an example) is consistent with these observations:

$$\text{Initiation step} \quad CH_2X_2 + h\nu \rightarrow CH_2X + X, \tag{1}$$

Recombination to produce isomer

$$CH_2X + X \rightarrow \text{iso-}CH_2X\text{–}X. \tag{2}$$

Reaction of iso-CH_2X–X with olefin

$$\text{iso-}CH_2X\text{–}X + \text{olefin} \rightarrow \text{cyclopropanated product} + X_2, \tag{3}$$

Formation of X_2–olefin complex

$$X_2 + \text{olefin} \Leftrightarrow X_2\text{–olefin complex}. \tag{4}$$

We have performed additional density functional theory computations to investigate the reaction of iso-CH_2Br–Br and ethylene as described in the Sec. III. The iso-CH_2Br–Br system was chosen since it is the smallest polyhalomethane we examined and therefore the most computationally tractable reaction to study. Figure 5 shows a simple schematic diagram outlining the reaction pathway for the iso-CH_2Br–Br with ethylene and CH_2Br with ethylene reactions with the transition state, intermediate, and product energies given relative to the separated reactants. The iso-CH_2Br–Br molecule approaches ethylene in an asymmetric way, preferentially attacking the CH_2 groups of ethylene from above the molecular plane. The chemical reaction computations indicate a complex is formed with the two intermolecular C–C distances of 3.258 Å and 3.772 Å and a binding energy of only 0.6 kcal/mol. A transition state (TS) is found on the way from this complex to the products of cyclopropane (C_3H_6) and Br_2. The C–C and C–Br bonds are lengthened by 0.023 Å and 0.086 Å and the Br–Br bond is shortened by 0.024 Å in the TS with respect to the reactant complex. The Br–Br–C angle changes from 126.7° in the reactant complex to 142.2° in TS. The structural changes are consistent with the fact that intermolecular interaction is much stronger in TS than in the complex, which results in the intramolecular C–C and C–Br bonds being weakened.

An imaginary frequency of 244.6(i) cm^{-1} was found for the TS structure by vibrational analysis. The eigenvector corresponding to the negative eigenvalue of the force constant

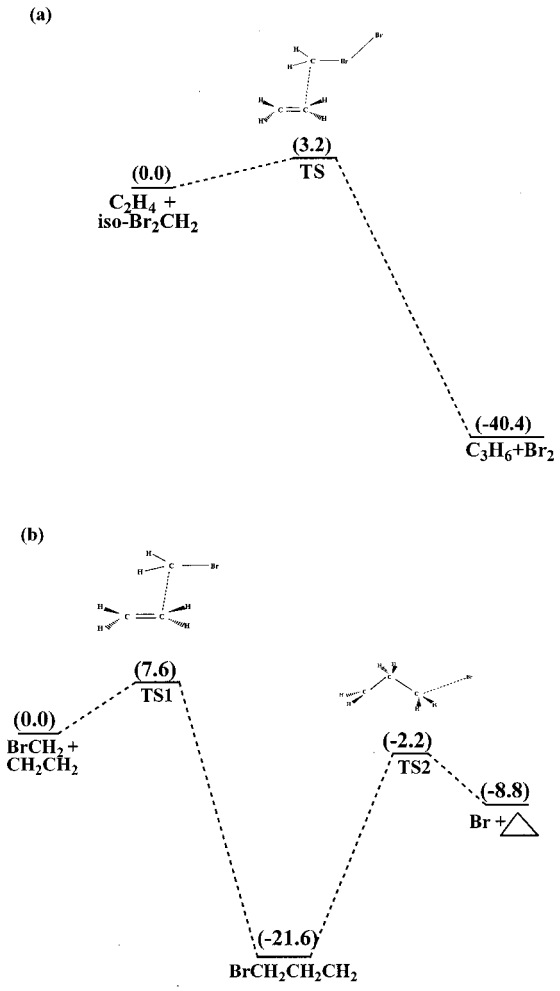

FIG. 5. Schematic diagram showing the UB3LYP/6-31+G* computed relative energies (in kcal/mol) for the reactants, transition state(s), intermediate, and reaction products for the reactions of iso-CH_2Br–Br with ethylene (a) and CH_2Br with ethylene (b). See text and EPAPS (Ref. 68) for more details. Selected computed structural parameters for the iso-CH_2Br–Br reaction with ethylene for TS: Br–Br=2.712 Å, C_3–Br=1.864 Å, C_1–C_2 =1.359 Å, C_3–C_2=2.226 Å, C_3–C_1=2.748 Å, Br–C_3–C_2=115.1°, Br–Br–C_3=142.2°, C_3–C_2–C_1=97.1°. Selected computed structural parameters for CH_2Br reaction with ethylene in (b): for TS1, C_3–Br =1.899 Å, C_1–C_2=1.359 Å, C_3–C_2=2.337 Å, Br–C–C=113.2°, C_3–C_2–C_1=106.5°; for intermediate, C_3–Br=1.981 Å, C_1–C_2=1.494 Å, C_3–C_2=1.535 Å, Br–C_3–C_2=112.1°, C_3–C_2–C_1=109.8°; for TS2, C_3–Br=2.422 Å, C_1–C_2=1.469 Å, C_3–C_2=1.498 Å, Br–C_3–C_2=106.7° and C_3–C_2–C_1=77.0°.

matrix indicates that the internal coordinate reaction vector is mainly composed of changes in the C–C intermolecular bond length and the Br–Br–C bond angle. The reaction vector has been identified as $0.41\,R_{C1-C3} + 0.56\,R_{C1-C2} - 0.22\,A_{Br-Br-C3}$. IRC calculations at the UB3LYP level confirm the transition state to connect the reactants of CH_2CH_2+iso-Br–Br–CH_2 and the products of $C_3H_6+Br_2$.

Relative to the separated reactants, the barrier height is calculated to be 3.2 kcal/mol with the zero-point correction. As pointed out before, an intermolecular complex is formed that has a stabilization energy of 0.6 kcal/mol. With respect to the zero-point level of the complex, the barrier becomes 3.8 kcal/mol. It is evident that the addition reaction between CH_2CH_2 and iso-Br–Br–CH_2 proceeds very easily, due to a

very small barrier on the way to products. Iso-Br–Br–CH_2 is an energetic molecule, and decomposition and isomerization of iso-Br–Br–CH_2 molecules may be in competition with the addition reaction. The CAS(10,8)/6-31+G* calculations show that the iso-Br–Br–CH_2 dissociation to $BrCH_2$+Br and CH_2+Br_2 are endothermic of 6.0 and 43.0 kcal/mol, respectively. Previous calculations[52] gave a barrier of about 10.0 kcal/mol for isomerization to CH_2Br_2. Therefore, we come to the conclusion that the cyclopropanation reaction is the dominant channel for iso-Br–Br–CH_2 in the presence of ethylene. Results for similar calculations for the CH_2Br radical with olefins have substantially larger barriers to reaction to give the cyclopropanated product. CH_2Br forms a very weak complex with ethylene and this complex has a barrier of 7.6 kcal/mol to form an intermediate Br–CH_2–CH_2–CH_2 which has a barrier of 19.6 kcal/mol to go on to the cyclopropanated product (C_3H_6) plus Br atom. These computational results show that the CH_2Br species has a very difficult route to give a cyclopropanated product while the iso-CH_2Br–Br species readily reacts with olefins to produce a cyclopropanated product (see Fig. 5). These preliminary computational results suggest that the iso-polyhalomethane species is most likely the methylene transfer agent (i.e., carbenoid species) responsible for cyclopropanation reactions via ultraviolet photoexcitation of polyhalomethanes in condensed phase environments in the presence of olefins. Further work is needed to better elucidate the chemical reactivity of the polyalomethane isomer in cyclopropanation reactions of olefins via ultraviolet photolysis of polyhalomethanes in solutions. We are currently using both experimental and theoretical methods to investigate these cyclopropanation reactions for olefins (via photoexcitation of polyhalomethanes in condensed phase environments) and results will be reported in due course.

D. Possible implications for release of reactive halogens in the troposphere and stratosphere

The iso-polyhalomethane species have an intense electronic absorption band in the 350–470 nm region that have much larger absorption coefficients in the ultraviolet–visible region than their parent polyhalomethanes. The iso-polyhalomethane absorption transitions are also significantly red-shifted compared to their parent polyhalomethane molecule. These two properties indicate that the iso-polyhalomethanes may be able to undergo further photochemical reactions in condensed phase environments in the atmosphere even though the iso-polyhalomethanes are transient species. It is known that ozone's (O_3) ultraviolet absorption spectrum is red-shifted in water and will photodissociate much more rapidly in water than in the gas phase.[71] The fact that the iso-polyhalomethane species readily reforms the parent molecule following visible light photoexcitation[41,42] in low temperature solids indicates that the X–X bond is broken following photoexcitation of the intense absorption band in the 350–470 nm region with release of a halogen atom. Whether or not these iso-polyhalomethane photochemical reactions are important in the atmosphere remains unknown at this time, but the increasing importance of multiphase and/or heterogeneous reactions in better understanding atmospheric chemistry[72–99] suggests that it would be worthwhile to explore the photochemistry of these iso-polyhalomethane species. We note that the lifetimes of these iso-polyhalomethanes would be expected to increase significantly as the temperature decreases and as the phase changes from liquid to solid.

In addition, the very reactive isomer–polyhalomethane species may undergo chemical reactions with olefins (such as alkenes, terpenes, and other volatile organic compounds found in the lower atmosphere)[100–109] and release a halogen molecule (X–X) as a product in cyclopropanation and/or other reactions (see Sec. IV C). Thus, formation of isomer–polyhalomethanes in condensed environments (such as water droplets and aerosol particles) may release reactive halogens into the atmosphere by both photochemical reactions and chemical reactions. Since so little is known about the photochemistry and chemistry of these intriguing iso-polyhalomethane species, it is not clear whether they will have any noticeable impact on the chemistry of the atmosphere. However, there are some recent observations that indicate the photochemistry of polyhalomethanes containing iodine and bromine does cause noticeable changes in the troposphere.[110] Iodine oxide (IO) was recently detected by long-path differential optical absorption spectroscopy (LP-DOAS) during the period of April 21 to May 30, 1997 in Mace Head, Ireland and the increased concentration of IO observed was linked to an increase in the concentration of CH_2I_2 and CH_2BrI and their photochemical reactions.[110] This suggests that it would be worthwhile to investigate whether the photochemistry of polyhalomethanes in condensed phase (i.e., multiphase and/or heterogeneous reactions) environments plays a role in the release of reactive halogens in the atmosphere. We are currently continuing our exploration of the identity, properties, photochemistry, and chemistry of these interesting iso-polyhalomethane species in different solvents (including water) and phases (both liquids and solids) using a variety of experimental and theoretical methods.

ACKNOWLEDGMENTS

This work was supported by grants from the Research Grants Council (RGC) of Hong Kong, the Committee on Research and Conference Grants (CRCG), and the Large Items of Equipment Allocation 1993–94 from the University of Hong Kong.

[1] Th. Class and K. Ballschmiter, J. Atmos. Chem. **6**, 35 (1988).
[2] S. Klick and K. Abrahamsson, J. Geophys. Res., [Oceans] **97**, 12683 (1992).
[3] K. G. Heumann, Anal. Chim. Acta **283**, 230 (1993).
[4] R. M. Moore, M. Webb, R. Tokarczyk, and R. Wever, J. Geophys. Res., [Oceans] **101**, 20899 (1996).
[5] L. Carpenter, East Atlantic Spring Experiment (EASE) 1997 campaign.
[6] J. C. Mössigner, D. E. Shallcross, and R. A. Cox, J. Chem. Soc., Faraday Trans. **94**, 1391 (1998).
[7] H. E. Simmons and R. D. Smith, J. Am. Chem. Soc. **81**, 4256 (1959).
[8] D. C. Blomstrom, K. Herbig, and H. E. Simmons, J. Org. Chem. **30**, 959 (1965).
[9] N. J. Pienta and P. J. Kropp, J. Am. Chem. Soc. **100**, 655 (1978).
[10] P. J. Kropp, N. J. Pienta, J. A. Sawyer, and R. P. Polniaszek, Tetrahedron **37**, 3229 (1981).
[11] P. J. Kropp, Acc. Chem. Res. **17**, 131 (1984).

[12] E. C. Friedrich, J. M. Domek, and R. Y. Pong, J. Org. Chem. **50**, 4640 (1985).
[13] E. C. Freidrich, S. E. Lunetta, and E. J. Lewis, J. Org. Chem. **54**, 2388 (1989).
[14] S. Durandetti, S. Sibille, and J. Pérchon, J. Org. Chem. **56**, 3255 (1991).
[15] J. M. Concellón, P. L. Bernad, and J. A. Pérez-Andrés, Tetrahedron Lett. **39**, 1409 (1998).
[16] M. Kawasaki, S. J. Lee, and R. Bersohn, J. Chem. Phys. **63**, 809 (1975).
[17] G. Schmitt and F. J. Comes, J. Photochem. **14**, 107 (1980).
[18] P. M. Kroger, P. C. Demou, and S. J. Riley, J. Chem. Phys. **65**, 1823 (1976).
[19] S. J. Lee and R. Bersohn, J. Phys. Chem. **86**, 728 (1982).
[20] L. J. Butler, E. J. Hintsa, and Y. T. Lee, J. Chem. Phys. **84**, 4104 (1986).
[21] L. J. Butler, E. J. Hintsa, and Y. T. Lee, J. Chem. Phys. **86**, 2051 (1987).
[22] G. Baum, P. Felder, and J. R. Huber, J. Chem. Phys. **98**, 1999 (1993).
[23] E. A. J. Wannenmacher, P. Felder, and J. R. Huber, J. Chem. Phys. **95**, 986 (1991).
[24] W. Radloff, P. Farmanara, V. Stert, E. Schreiber, and J. R. Huber, Chem. Phys. Lett. **291**, 173 (1998).
[25] S. R. Cain, R. Hoffman, and R. Grant, J. Phys. Chem. **85**, 4046 (1981).
[26] K.-W. Jung, T. S. Ahmadi, and M. A. El-Sayed, Bull. Korean Chem. Soc. **18**, 1274 (1997).
[27] S. L. Baughcum, H. Hafmann, S. R. Leone, and D. Nesbitt, Faraday Discuss. Chem. Soc. **67**, 306 (1979).
[28] S. L. Baughcum and S. R. Leone, J. Chem. Phys. **72**, 6531 (1980).
[29] J. Zhang and D. G. Imre, J. Chem. Phys. **89**, 309 (1988).
[30] J. Zhang, E. J. Heller, D. Huber, D. G. Imre, and D. Tannor, J. Chem. Phys. **89**, 3602 (1988).
[31] W. M. Kwok and D. L. Phillips, Chem. Phys. Lett. **235**, 260 (1995).
[32] W. M. Kwok and D. L. Phillips, J. Chem. Phys. **104**, 2529 (1996).
[33] W. M. Kwok and D. L. Phillips, J. Chem. Phys. **104**, 9816 (1996).
[34] S. Q. Man, W. M. Kwok, and D. L. Phillips, J. Phys. Chem. **99**, 15705 (1995).
[35] S. Q. Man, W. M. Kwok, A. E. Johnson, and D. L. Phillips, J. Chem. Phys. **105**, 5842 (1996).
[36] F. Duschek, M. Schmitt, P. Vogt, A. Materny, and W. Kiefer, J. Raman Spectrosc. **28**, 445 (1997).
[37] M. Braun, A. Materny, M. Schmitt, W. Kiefer, and V. Engel, Chem. Phys. Lett. **284**, 39 (1998).
[38] X. Zheng and D. L. Phillips, Chem. Phys. Lett. **313**, 467 (1999).
[39] J. P. Simons and P. E. R. Tatham, J. Chem. Soc. A **1966**, 854.
[40] H. Mohan, K. N. Rao, and R. M. Iyer, Radiat. Phys. Chem. **23**, 505 (1984).
[41] G. Maier and H. P. Reisenauer, Angew. Chem. Int. Ed. Engl. **25**, 819 (1986).
[42] G. Maier, H. P. Reisenauer, J. Lu, L. J. Scaad, and B. A. Hess, Jr., J. Am. Chem. Soc. **112**, 5117 (1990).
[43] L. Andrews, F. T. Prochaska, and B. S. Ault, J. Am. Chem. Soc. **101**, 9 (1979).
[44] H. Mohan and R. M. Iyer, Radiat. Eff. **39**, 97 (1978).
[45] H. Mohan and P. N. Moorthy, J. Chem. Soc., Perkin Trans. **2**, 277 (1990).
[46] B. J. Schwartz, J. C. King, J. Z. Zhang, and C. B. Harris, Chem. Phys. Lett. **203**, 503 (1993).
[47] K. Saitow, Y. Naitoh, K. Tominaga, and Y. Yoshihara, Chem. Phys. Lett. **262**, 621 (1996).
[48] A. N. Tarnovsky, J.-L. Alvarez, A. P. Yartsev, V. Sündstrom, and E. Åkesson, Chem. Phys. Lett. **312**, 121 (1999).
[49] X. Zheng and D. L. Phillips, J. Phys. Chem. A **104**, 6880 (2000).
[50] X. Zheng and D. L. Phillips, Chem. Phys. Lett. **324**, 175 (2000).
[51] X. Zheng and D. L. Phillips, J. Chem. Phys. **113**, 3194 (2000).
[52] X. Zheng, W. M. Kwok, and D. L. Phillips, J. Phys. Chem. A **104** (2000, in press).
[53] D. Pan, L. C. T. Shoute, and D. L. Phillips, Chem. Phys. Lett. **303**, 629 (1999).
[54] D. Pan and D. L. Phillips, J. Phys. Chem. A **103**, 4737 (1999).
[55] D. Pan, L. C. T. Shoute, and D. L. Phillips, J. Phys. Chem. A **103**, 6851 (1999).
[56] D. Pan, L. C. T. Shoute, and D. L. Phillips, Chem. Phys. Lett. **316**, 395 (2000).
[57] M. J. Frisch, G. W. Trucks, H. B. Schlegel *et al.*, GAUSSIAN 98, Revision A.7 (Gaussian, Inc., Pittsburgh, Pennsylvania, 1998).
[58] A. D. Becke, J. Chem. Phys. **98**, 1372 (1993).
[59] R. Bauernschmitt and R. Ahlrichs, Chem. Phys. Lett. **256**, 454 (1996).
[60] T. H. Dunning, Jr., J. Chem. Phys. **90**, 1007 (1989).
[61] A. K. Wilson, D. E. Woon, K. A. Peterson, and T. H. Dunning, Jr., J. Chem. Phys. **110**, 7667 (2000). Basis sets were obtained from the Extensible Computational Chemistry Environment Basis Set Database, Version 1.0, as developed and distributed by the Molecular Science Computing Facility, Environmental and Molecular Sciences Laboratory which is part of the Pacific Northwest Laboratory, P.O. Box 999, Richland, Washington 99352, U.S.A. and funded by the U.S. Department of Energy. The Pacific Northwest Laboratory is a multi-program laboratory operated by Battelle Memorial Institute for the U.S. Department of Energy under Contract No. DE-AC06-76RLO 1830. Contact David Feller or Karen Schuchardt for further information.
[62] N. Godbout, D. R. Salahub, J. Andzelm, and E. Wimmer, Can. J. Chem. **70**, 560 (1992). Basis sets were obtained from the Extensible Computational Chemistry Environment Basis Set Database, Environmental and Molecular Sciences Laboratory which is part of the Pacific Northwest Laboratory, P.O. Box 999, Richland, Washington 99352, U.S.A., and funded by the U.S. Department of Energy. The Pacific Northwest Laboratory is a multi-program laboratory operated by Battele Memorial Institute for the U.S. Department of Energy under Contract No. DE-AC06-76RLO 1830. Contact David Feller or Karen Schuchardt for more information.
[63] A. J. Sadlej, Theor. Chim. Acta **81**, 339 (1992).
[64] F. Bernardi, A. Bottini, J. J. W. McDougall, M. A. Robb, and H. B. Schlegel, Faraday Symp. Chem. Soc. **19**, 137 (1984).
[65] M. J. Frisch, I. N. Ragazos, M. A. Robb, and H. B. Schlegel, Chem. Phys. Lett. **189**, 524 (1992).
[66] C. Gonzalez and H. B. Schlegel, J. Chem. Phys. **90**, 2154 (1989).
[67] N. Yamamoto, T. Vreven, M. A. Robb, M. J. Frisch, and H. B. Schlegel, Chem. Phys. Lett. **250**, 373 (1996).
[68] See EPAPS document No. E-JCPSA6-113-001048 for supporting information on density functional theory calculation results. This document may be retrieved via the EPAPS homepage (http://www.aip.org/pubservs/epaps.html) or from ftp.aip.org in the directory /epaps/. See the EPAPS homepage for further information.
[69] X. Zheng and D. L. Phillips, Chem. Phys. Lett. **316**, 524 (2000).
[70] G. P. Brown and J. P. Simons, Trans. Faraday Soc. **65**, 3245 (1969).
[71] M. S. Kharasch, E. V. Jensen, and W. H. Urry, J. Am. Chem. Soc. **69**, 1100 (1947).
[72] H. Taube, Trans. Faraday Soc. **53**, 656 (1957).
[73] M. J. Molina, T. L. Tso, L. T. Molina, and F. C. Y. Wang, Science **238**, 1253 (1987).
[74] M. A. Tolbert, M. J. Rossi, and D. M. Golden, Science **240**, 1018 (1988).
[75] D. Hanson and K. Mauersberger, Geophys. Res. Lett. **15**, 855 (1988).
[76] D. Hofmann, Nature (London) **337**, 447 (1989).
[77] J. Lelieveld and P. J. Crutzen, Nature (London) **343**, 227 (1990).
[78] M. J. Molina, Atmos. Environ. A **25**, 2535 (1991).
[79] D. R. Hanson and A. R. Ravishankara, J. Phys. Chem. **96**, 2682 (1992).
[80] G. Brasseur and C. Granier, Science **257**, 1239 (1992).
[81] M. J. Prather, J. Geophys. Res. **97**, 10187 (1992).
[82] F. J. Dentener and P. J. Crutzen, J. Geophys. Res. **98**, 7149 (1993).
[83] D. R. Hanson, A. R. Ravishankara, and S. Solomon, J. Geophys. Res. **99**, 3615 (1994).
[84] T. Koop and K. S. Carslaw, Science **272**, 1638 (1996).
[85] M. A. Tolbert, Science **272**, 1597 (1996).
[86] J. Reichardt, A. Ansmann, M. Serwazi, C. Weitkamp, and W. Michaelis, Geophys. Res. Lett. **23**, 1929 (1996).
[87] R. Vogt, P. J. Crutzen, and R. Sander, Nature (London) **383**, 327 (1996).
[88] D. Davis, J. Crawford, S. Liu *et al.*, J. Geophys. Res., [Oceans] **101**, 2135 (1996).
[89] J. P. D. Abbatt, Geophys. Res. Lett. **24**, 1479 (1997).
[90] M. O. Andrqe and P. J. Crutzen, Science **221**, 744 (1997).
[91] B. J. Finlayson-Pitts and J. N. Pitts, Jr., Science **276**, 1045 (1997).
[92] A. R. Ravishankara, Science **276**, 1051 (1997).
[93] L. J. Liang and D. J. Jacob, J. Geophys. Res., [Oceans] **102**, 5993 (1997).
[94] C. J. Walcek, H.-H. Yuan, and W. R. Stockwell, Atmos. Environ. **31**, 1221 (1997).
[95] K. W. Oum, M. J. Lakin, D. O. DeHaan *et al.*, Science **279**, 74 (1998).
[96] N. A. Clegg and R. Toumi, J. Geophys. Res., [Oceans] **103**, 31095 (1998).
[97] L. J. Carpenter, W. T. Sturges, S. A. Penkett *et al.*, J. Geophys. Res., [Oceans] **104**, 1679 (1999).
[98] B. Ramacher, J. Rudolph, and R. Koppmann, J. Geophys. Res., [Oceans] **104**, 3633 (1999).

[99] R. Vogt, R. Sander, R. Von Glasow, and P. J. Crutzen, J. Atmos. Chem. **32**, 375 (1999).
[100] *Chemistry of Atmospheres*, 3rd ed., edited by R. P. Wayne (Oxford University Press, Oxford, 2000).
[101] H. Niki, P. D. Maker, C. M. Savage, and L. P. Breitenbach, Environ. Sci. Technol. **17**, 312A (1983).
[102] S. Hatakeyama, K. Izumi, T. Fukuyama, and H. Akimoto, J. Geophys. Res., [Oceans] **94**, 13013 (1989).
[103] P. Neeb, O. Horie, and G. K. Moortgat, Chem. Phys. Lett. **246**, 150 (1995).
[104] A. A. Chew and R. Atkinson, J. Geophys. Res., [Oceans] **101**, 28649 (1996).
[105] N. J. Blake, D. R. Blake, T.-Y. Chen *et al.*, J. Geophys. Res., [Oceans] **102**, 28315 (1997).
[106] D. Helmig, J. Greenberg, A. Guenther *et al.*, J. Geophys. Res., [Oceans] **103**, 22397 (1998).
[107] N. M. Donohue, J. H. Kroll, J. G. Anderson, and K. L. Demerjian, Geophys. Res. Lett. **25**, 59 (1998).
[108] T. Pfeiffer, O. Forberich, and F. J. Comes, Chem. Phys. Lett. **298**, 351 (1998).
[109] S. Houweling, F. Dentener, and J. Lelieveld, J. Geophys. Res., [Oceans] **103**, 10673 (1998).
[110] B. Alicke, K. Hebestreit, J. Stutz, and U. Platt, Nature (London) **397**, 572 (1999).